Phase separation of co-solvent promotes multiple bio-nanomaterials conversion from natural lignocellulose

Si Mengying, Sillanpää Mika, Zhuo Shengnan, Zhang Jin, Liu Mingren, Wang Sheng, Gao Congjie, Chai Liyuan, Zhao Feiping, Shi Yan

DOI: 10.1016/j.indcrop.2020.112469

Contents lists available at ScienceDirect

Industrial Crops & Products

journal homepage: www.elsevier.com

Phase separation of co-solvent promotes multiple bio-nanomaterials conversion from natural lignocellulose

Mengying Si [a, b], Mika Sillanpää [c], Shengnan Zhuo [a], Jin Zhang [d], Mingren Liu [a], Sheng Wang [b], Congjie Gao [a, e], Liyuan Chai [a, b], Feiping Zhao [a, b, c, *], Yan Shi [a, b, *]

[a] School of Metallurgy and Environment, Central South University, Changsha 410083, China
[b] Chinese National Engineering Research Centre for Control & Treatment of Heavy Metal Pollution, Changsha 410083, China
[c] Department of Green Chemistry, School of Engineering Science Lappeenranta-Lahti University of Technology, Mikkeli FI-50170, Finland
[d] College of Environmental Science and Engineering, Hunan University, Changsha 410082, China
[e] Water Treatment Technology Development Center, Zhejiang University of Technology, Hangzhou 310014, China

ARTICLE INFO

Keywords:
Phase separation
Lignocellulose structure
Bio-nanomaterials conversion
Lignin nanoparticles (LNPs)
Microfibrillated celluloses (MFCs)
Carbon quantum dots (CQDs)

ABSTRACT

Natural lignocellulose is supported by parallel bundles of cellulose (framework) and contains tightly interlaced hemicellulose and lignin. Based on the heterogeneous structure, an acid-catalyzed tetrahydrofuran–water (THF–H_2O) co-solvent system was designed for the preparation of multiple bio-nanomaterials from natural lignocellulose, including microfibrillated celluloses (MFCs), lignin nanoparticles (LNPs), and carbon quantum dots (CQDs). In this setting, the phase separation of the co-solvent on the surface of lignocellulose enhanced the component fractionation. 95.6% of lignin with high content of G units was effectively removed from the lignocellulose matrix mainly by cleaving β–O–4 bonds to form uniformly spherical LNPs via π–π interactions. The obtained monodisperse LNPs with the average size of 102 nm contained a low ratio of S/G, relatively high content of C – C linkages and abundant functional groups, which exhibited high stability and application value. Meanwhile, 89.1% of the hemicellulose were hydrolyzed to retain a high content of cellulose in lignocellulose residues. Then the MFCs with slender fibrils of approximately 150 nm in diameter were liberated from the cellulose bundles in lignocellulose residues. The released monomolecular compounds, which served as precursors, were thermally processed for CQDs production. This study integrates three types of lignocellulose-based nanomaterial preparation into an integrated pathway to greatly promote the industrialization process of bio-nanomaterials.

1. Introduction

Lignocellulose consists of 40%–50% cellulose, 25%–30% hemicellulose, 15%–20% lignin, and other extractable components (Lynd et al., 2008, 2017; Si et al., 2019). Nature purposely designs the microstructure of the lignocellulosic polymers to serve as a structural component embedded in cell walls of plants, protecting it from deconstruction. Nevertheless, this inherently recalcitrant cell wall envelops various latent bio-nanomaterials, which have the potential to play important roles in addressing the challenges of the impending environmental and energy crisis (Ragauskas et al., 2014; Zhu et al., 2016).

As a principal framework of the cell wall, cellulose is an unbranched homo-polyglucan, primarily linked by glycosidic bonds (β–1,4 linkages) (Abdul Khalil et al., 2012). Intrachain hydrogen bonding between oxygens and hy-

Abbreviations: CS, Corn Stover; THF, Tetrahydrofuran; THF–H_2O, Tetrahydrofuran–Water; LNP, Lignin Nanoparticle; MFC, Microfibrillated Cellulose; CQD, Carbon Quantum Dot; S, Syringyl Units; G, Guaiacyl Units; H, p-hydroxyphenyl Units; CrI, Crystallinity Index; TL, Treatment Liquor.

* Corresponding authors at: School of Metallurgy and Environment, Central South University, Changsha 410083, China.
Email addresses: feiping.zhao@lut.fi (F. Zhao); shiyzyrs@csu.edu.cn (Y. Shi)

https://doi.org/10.1016/j.indcrop.2020.112469
Received 31 January 2020; Received in revised form 7 April 2020; Accepted 10 April 2020
Available online xxx
0926-6690/

Table 1
Characterization of the lignin fractions in CS and TL by GPC and HSQC.

Sample	CS	TL
M_w (Daltons)	3442	3172
M_n (Daltons)	426	1466
PDI	7.92	2.16

droxyl groups of adjacent ring molecules stabilizes the linkages and promotes the formation of the linear configuration of cellulose. Multiple parallel stacking of linear cellulose chains (generally 36 in quantity) form elementary fibrils (3 nm in diameter) by van der Waals forces and intermolecular hydrogen bonding between the oxygens and hydroxyl groups of adjacent molecules, subsequently aggregating into larger microfibrils (Atalla and DL, 1984; Ding and Himmel, 2006; Moon et al., 2011). Recently, several cellulosic nanomaterials, such as nanocellulose, nanofibrils, and whiskers, were derived from these microfibrils and classified as either microfibrillated celluloses (MFCs) (Jia et al., 2018) or cellulose nanocrystals (CNCs) (Parker et al., 2018; Zhang and Liimatainen, 2018) depending on the preparation method (Kontturi et al., 2018; Rajinipriya et al., 2018). Because of their "green" characteristics, including compatibility, degradability, and sustainability, nanocelluloses have been considered as alternatives to conventional hazardous colorants applied in textiles, cosmetics, sensing, art, and food (Guidetti et al., 2016; Parker et al., 2018). However, in the natural structure, the intra- and inter-chain hydrogen bonding gives these parallel microfibrils high axial stiffness (Kai et al., 2016). The interlaced hemicellulose and lignin form a matrix to encapsulate cellulose microfibrils into bundles for embedding in the cell wall (Kontturi et al., 2018), inhibiting the separation of the microfibrils.

Thereinto, lignin, an energy-dense alkyl-aromatic polymer, is crucial for the integrity of the cell wall structure and

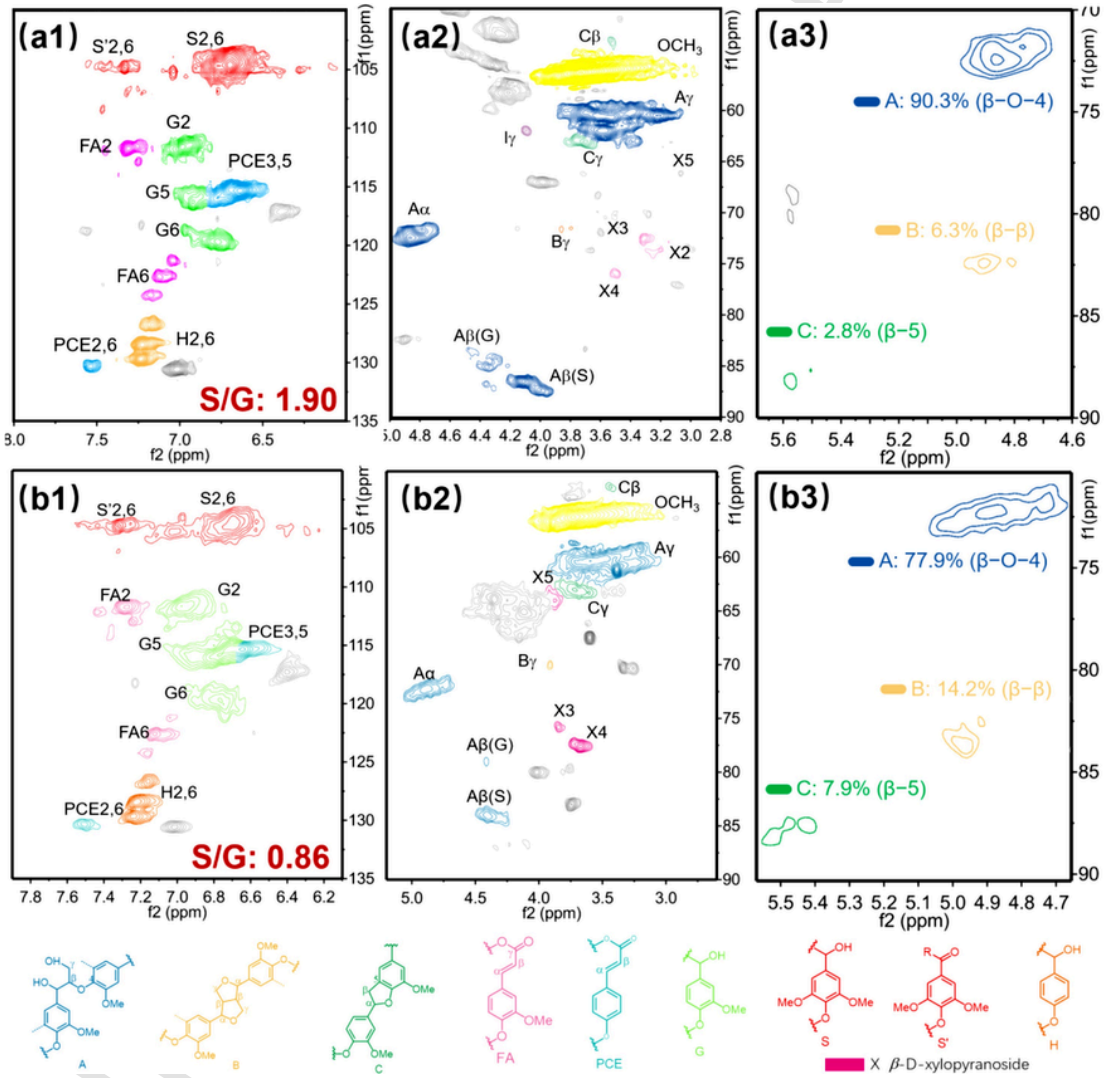

Fig. 1. HSQC spectra of the lignin fractions in natural CS and TL. Aromatic region (a1) and side-chain region (a2 and a3) of the lignin in untreated CS; aromatic region (b1) and side-chain region (b2 and b3) of the lignin in TL. (A) *β*-O-4 alkyl-aryl ethers; (B) resinols; (C) phenylcoumaran; (I) p-hydroxycinnamoyl alcohol end groups; (FA) ferulates; (PCE) p-coumarates; (S) syringyl units; (S′) oxidized syringyl units bearing a carbonyl at C; (G) guaiacyl units; (H) para-hydroxy-phenyl units; (X) β-D-xylopyranoside. S/G ratio obtained by S/G ratio = $0.5I_{S2,6}/I_{G2}$; Bond content obtained using $Ix\% = Ix/(I_A + I_B + I_C) \times 100\%$; I_A, I_B, I_C represent the *α*-position signal of *β*-O-4, *β*-*β*, and *β*-5, respectively.

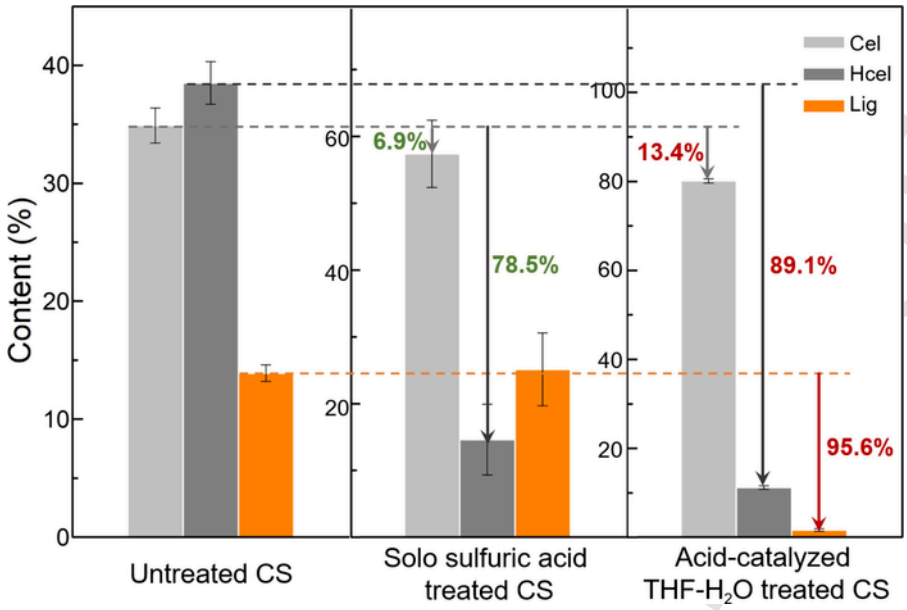

Fig. 2. The effect of acid-catalyzed treatment on the chemical composition of CS; Cel: cellulose, Hcel: hemicellulose, Lig: lignin.

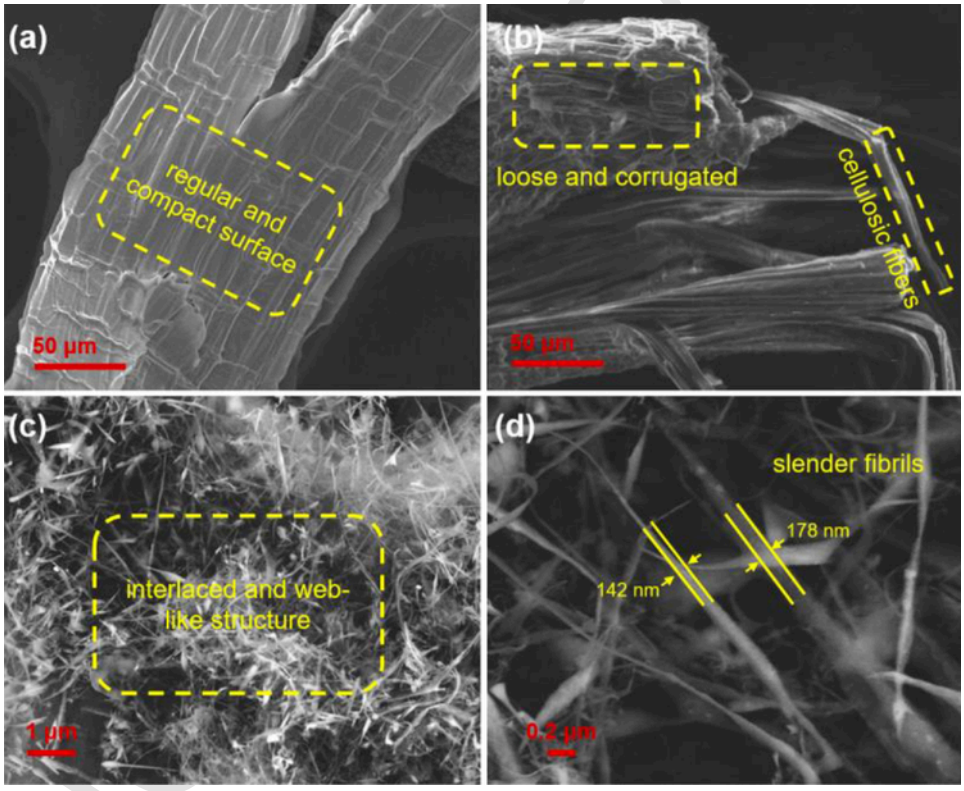

Fig. 3. SEM images of the untreated CS (a), treated CS residues (b), and MFCs (c–d).

stiffness of the stem (Ago et al., 2016). Lignin is composed of three monolignols including guaiacyl G, syringyl S, and p-hydroxyphenyl H phenylpropanoid units which are linked by aryl ether (e.g., *β*–O–4, *α*–O–4) and carbon – carbon (C – C) bonds (e.g., *β*–5, *β*–*β*, 5–5) (Zhao et al., 2016). Recent research suggests that lignin has emerged as a substitute for toxic nanomaterials in form of lignin nanoparticles (LNPs) (Kai et al., 2016; Richter et al., 2015). The LNPs-based composites can be fabricated by introducing functional groups into the lignin matrix and applied in UV barrier enhancement, drug delivery, and enhancement of antibacterial and antioxidant properties (Figueiredo et al., 2018; Lintinen et al., 2018; Si et al., 2018b). In addition, recent studies have shown that zero-dimensional carbon quantum dots (CQDs) can be prepared from lignocellulosic component such as glucose (Yang et al., 2011), lignin (Niu et al., 2017), protein (Wang et al., 2012), and other natural biomass (Zhang et al.,

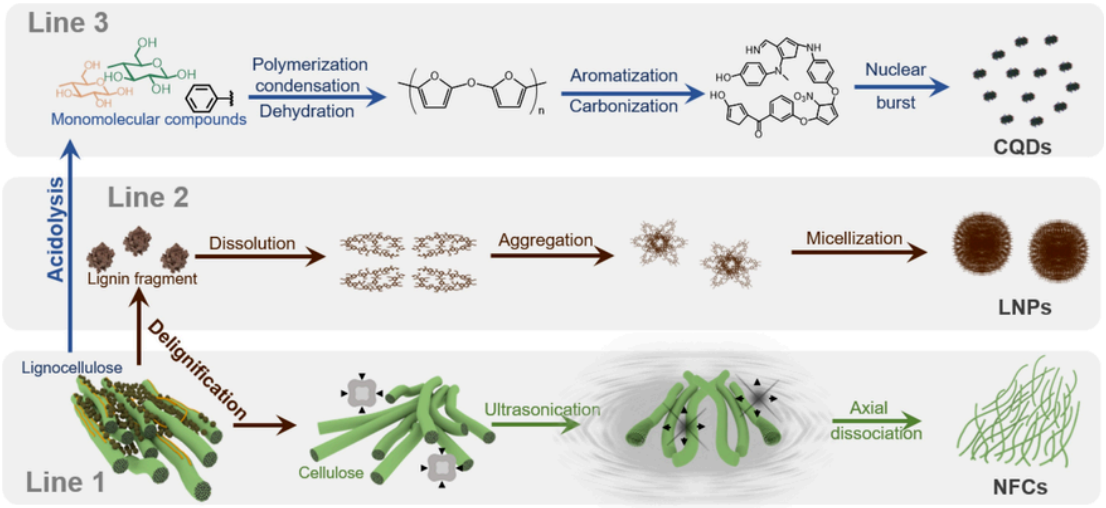

Fig. 4. The formation mechanism of the bio-nanomaterials.

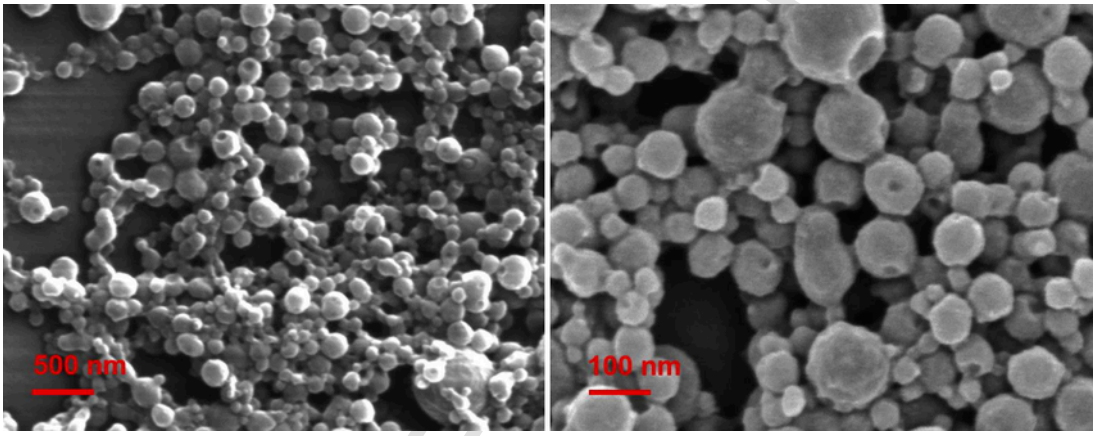

Fig. 5. SEM images of the LNPs.

Table 2
Characterization of the LNPs by XPS and HSQC.

XPS	C/O	C 1s		
		C–C [a]	C–O [b]	C = O [c]
	3.53	65.4	27.7	6.9
HSQC	S/G/H	Linkages		
		β–O–4	*β*–*β*	*β*–5
	0.86/1/0.53	77.9	14.2	7.9

[a] C-C = $A_{C\text{-}C}/(A_{C\text{-}C}+A_{C\text{-}O}+A_{C=O})$; $A_{C\text{-}C}$: the peak area of the C–C in C 1s spectrum, $A_{C\text{-}O}$: the peak area of the C–O in the C 1s spectrum, $A_{C=O}$: the peak area of the C = O in the C 1s spectrum.

[b] C-O = $A_{C\text{-}O}/(A_{C\text{-}C}+A_{C\text{-}O}+A_{C=O})$; $A_{C\text{-}C}$: the peak area of the C–C in the C 1s spectrum, $A_{C\text{-}O}$: the peak area of the C–O in the C 1s spectrum, $A_{C=O}$: the peak area of the C = O in the C 1s spectrum.

[c] C = O = $A_{C\text{-}O}/(A_{C\text{-}C}+A_{C\text{-}O}+A_{C=O})$; $A_{C\text{-}C}$: the peak area of the C–C in the C 1s spectrum, $A_{C\text{-}O}$: the peak area of the C–O in the C 1s spectrum, $A_{C=O}$: the peak area of the C = O in the C 1s spectrum.

2018c). The as-prepared CQDs show value-added applicability in bioimaging, sensors, and drug delivery, because of their optical properties and fluorescent emissions (Lim et al., 2015; Zhang et al., 2018a).

Accelerating energy consumption breeds the unprecedented urgency of developing these bio-nanomaterial technologies (Almeida et al., 2018). However, the heterogeneous and highly crosslinked structure is a challenge for advanced material fabrication from natural lignocellulose, and generating these bio-nanomaterial preparations generally involves complex processing. Generally, a rigorously tedious chemical process, mainly including Soxhlet extraction and bleaching to fractionate lignin and hemicellulose from lignocellulose, is indispensable (Thomas et al., 2018). Besides, most of the preparation studies involved single material or two at most (Dou et al., 2019; Si et al., 2018b). The consequent increase of the input inevitably limits the industrial application of the bio-nanomaterials. Therefore, efficient fractionation and preparation techniques are needed to liberate various components from the recalcitrant matrix for fabrication of bionanomaterials.

Tetrahydrofuran (THF), a biomass derivative, is particularly appealing for the sustainable bioindustry because of its easy recoverability arising from its low boiling point. In a tetrahydrofuran–water (THF–H_2O) co-solvent, THF molecules generally stack on the hydrophobic areas, and H_2O molecules form hydrogen bonding with the hydrophilic faces, resulting in phase separation (Mostofian et al., 2016). Herein, an acid-catalyzed THF–H_2O co-solvent system was performed, where corn stover (CS) was employed as a natural biomass source, and sulfuric acid initiated polysaccharide hydrolysis and lignin depolymerization. The

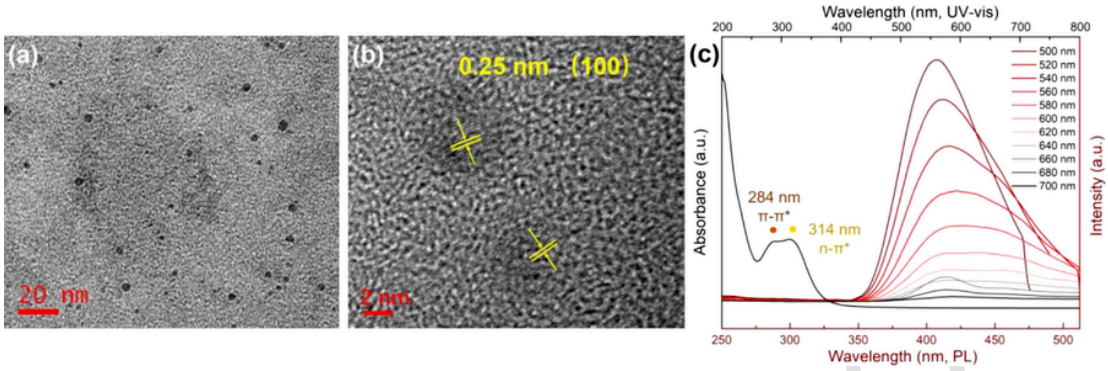

Fig. 6. a) and (b) TEM images of CQDs. (c) UV–vis absorption (left) and PL emission spectra (right) of the CQDs at different excitation wavelengths.

phase separation in the THF–H_2O co-solvent system was conducted to enhance the multiple bionanomaterials preparation from the natural lignocellulose. In detail, the lignin and cellulose were fractionated in the presence of the THF–H_2O co-solvent system. The THF-dissolved lignin was expected to form nanoparticles. The cellulose microfibrils, in the form of MFCs, were easily liberated from the cellulose by mechanical breakdown. Concomitantly, the depolymerized monomolecular compounds served as the precursors for thermal preparation of CQDs via dehydration, polymerization, condensation, aromatization, and carbonization. Our study provides an efficient platform to integrate three types of lignocellulose-based nanomaterial preparation into a unitary pathway.

2. Materials and method

2.1. Materials

The corn stover (CS) powder was obtained from Shandong Province, China and sifted using a 60-mesh griddle. Then the air-dried CS powder was used as the natural material. The tetrahydrofuran (THF) was purchased from Macklin Biochemical Co., Ltd (Shanghai, China). Sulfuric acid (H_2SO_4, 98 wt%) was purchased from Guangfu, Tianjin, China. The alkali lignin was purchased from Sigma–Aldrich.

2.2. THF–H_2O co-solvent system treatment

Experimental flow was shown in Scheme S1. In detail, 3 g of air-dried CS was mixed with 60 mL of THF-H_2O solution (1:1, v/v) containing 0.1 mol/L H_2SO_4, as previous reported (Nguyen et al., 2015, 2017; Nguyen et al., 2016). Generally, a thermochemical treatment that exceeds the glass transition temperature of lignin (around 120 °C (Sen et al., 2015; Thakur et al., 2014)) allows them to expand and become mobile within the cell wall matrix (Donohoe et al., 2008). Herein, we aimed to initiate the melt of the depolymerized lignin fragments to expand out of the cell wall matrix. Therefore, the mixture was transferred into a 100-mL stainless steel kettle body with a Teflon liner and statically heated in a blast drying oven (101-A1, Marit) at 120 °C for 2 h. A solo sulfuric acid treatment was performed in the distilled water containing 0.1 mol/L (1.0 wt%) H_2SO_4 under the same conditions as the control group. After the reaction finished, the reactor was naturally cooled off to room temperature. 25-fold volume of water was added to stop the reaction. The mixture was filtered through multi-layer gauze to separate the colloidal solution and the treated CS residues. The CS residues were collected and thoroughly washed with de-ionized water.

The collected CS residues were immersed in de-ionized water to fabricate microfibrillated celluloses (MFCs) by sonication. The ultrasonication was performed at 60 kHz and 400 W with a Sonic Ruptor (OMNI Sonic Ruptor 400, USA), repeating the cycle of 0.4 s ultrasonic treatment and 0.4 s shutdown. The ultrasonic circulation lasted for 1 h (Lu et al., 2013). Then, the mixture was centrifuged at 5000 rpm for 5 min to collect the MFCs. The colloidal solution was centrifuged at the relative centrifugal force of 24,000 *g* to separate LNPs and CQDs. After centrifugation, the precipitate was the LNPs. The CQDs dispersed in the supernatant liquor (Si et al., 2018b). The LNPs were obtained by freeze-drying the precipitate.

2.3. Characterization of the CS residue

The weight of CS before and after treatment was accurately measured. The weight loss during the treatment was calculated according to the Eq. (1) below. The chemical composition of CS was determined as described by Teramoto et al. (2008). Then, the removal of the constituents was calculated according to Eqs. (2)–(4) below.

$$W_{,\%} = (M_1\text{-}M_2) / M_1 \quad (1)$$

$$Q_{lig} = [C_{lig} \bullet M_1 - C'_{lig} \bullet M_2] / C_{lig} \bullet M_1 \quad (2)$$

$$Q_{cel} = [C_{cel} \bullet M_1 - C'_{cel} \bullet M_2] / C_{cel} \bullet M_1 \quad (3)$$

$$Q_{hcel} = [C_{hcel} \bullet M_1 - C'_{hcel} \bullet M_2] / C_{hcel} \bullet M_1 \quad (4)$$

where W is the weight loss of CS during the treatment; M_1 is the weight of the natural CS; and the M_2 is the weight of treated CS. Q_{lig}, Q_{cel}, and Q_{hcel} are the removal of the lignin, cellulose, and hemicellulose, respectively; C_{lig}, C_{cel}, and C_{hcel} are the contents of lignin, cellulose, and hemicellulose in the natural CS, repectively; and C'_{lig}, C'_{cel}, and C'_{hcel} are the contents of lignin, cellulose, and hemicellulose in the treated CS, respectively.

The morphology of CS was detected by scanning electron microscopy (SEM, JSM-IT300LA, JEOL, Japan). A 1760X Fourier transform infrared (FTIR) spectrometer (NICOLET IS10, Thermo, U.S.A) and X-ray diffractometry (XRD, Bruker D8 Advance) were employed to analyze the

structure of CS (Si et al., 2018a). The crystallinity index of CS was calculated using the Eq. 5 (Segal, 1959).

$$CrI = (I_{002} - I_{amp}) / I_{002} \quad (5)$$

where CrI is the crystallinity index of CS; I_{002} is the intensity of the peak at $2\theta = 22.4^{\circ}$ and I_{amp} is the background intensity at $2\theta = 15.6^{\circ}$.

The lignin was extracted from the natural CS and the treatment liquor (Wen et al., 2015). Then, the gel permeation chromatography (GPC, Waters 1515, USA) and heteronuclear single quantum coherence (HSQC)–nuclear magnetic resonance (NMR, Bruker GmbH, Karlsruhe, Germany) were employed to analyze the molecular weight and structure of the lignin (Cai et al., 2016; Linger et al., 2014). The monosaccharide in the treatment liquor (TL) was analyzed by the high-performance liquid chromatography (HPLC) system (Agilent 1200, China) equipped with a refractive index (RI) detector (Agilent G1362A, China) (Dai et al., 2015). Furthermore, the TL was acidified to pH 2.0 and extracted with ethyl acetate repeatedly. Then, the extraction was analyzed by GC QP2010 MS (Shimadzu, Kyoto, Japan) (Shi et al., 2013).

2.4. Characterization of bio-nanomaterial

The solid MFCs were coated with gold and then observed under a scanning electron microscope (SEM, JSM-IT300LA, JEOL, Japan). The X-ray diffractometry and FTIR spectrometry were performed to explore the structure of the MFCs. A Helios NanoLab (Helios Nanolab G3 UC, FBI, U.S.A) was employed to observed the morphology of LNPs. The structure of the LNPs was analyzed by FTIR spectrometry, X-ray diffractometry, and X-ray photo-electron spectroscopy (XPS, ESCALAB 250Xi, Thermo Fisher Scientific). HSQC and ^{31}P NMR spectra of the LNPs were performed in a Bruker Avance 400 MHz spectrometer (Bruker GmbH, Karlsruhe, Germany). Furthermore, UV–vis spectroscopy (U-4100, Hitachi, Japan) analysis was employed to further explore the formation mechanism of the LNPs. The alkali lignin and dissolved lignin were characterized as the controls. The CQDs were observed under TEM and high-resolution TEM. Then FTIR spectrometer, XPS and Raman spectra (Renishaw Raman system model 1000 spectrometer with radiation at 633 nm) were employed to analyze the structure of the CQDs. Photoluminescence (PL) spectra were performed using a fluorescence spectrophotometer (Edinburgh FLsp920 transient, USA). The Zeta potential of the CQDs at pH 2–11 was measured via a Malvern Zetasizer Nano-ZS ZEN3600 Instrument (Malvern, United Kingdom).

3. Results and discussion

3.1. Delignification in treatment

Thermochemical treatment generally modifies the lignin in lignocellulose. Herein, CS was selected as the natural material and treated in an acid-catalyzed tetrahydrofuran–water (THF–H_2O) co-solvent system. The structure of lignin in the untreated CS and treatment liquor (TL) were analyzed via GPC, GC-MS, and HSQC. As shown in Table 1, the lignin fraction in CS exhibits a slightly larger M_w (3443 Da) as compared with the lignin in TL (3172 Da), suggesting that some sensitive linkages of the macromolecular lignin in CS were cleaved during the treatment. Meanwhile, the M_n of lignin in CS (426 Da) sharply increases to 1466 Da, accompanied by a significant decrease in polydispersity (PDI, decrease from 7.92 to 2.16). These results indicated that the micromolecule lignin might be completely deconstructed, which was well confirmed by the GC-MS results (Figure S1). The exhibited glycol, glyoxylic acid, phenylacetic acid, 2,6-dihydroxy-benzoic acid, 2-hydroxy-3-methyl-benzoic acid, and 3-methyl-2-furoicacid might be attributed to the lignin degradation (Shi et al., 2013; Zhang et al., 2015). The HSQC analysis generally generates important structural information on the lignin macromolecule. Fig. 1 presents the explicit structural evolution of lignin during the treatment. The S/G ratio significantly decreases from 1.90 to 0.86, indicating that the G type lignin is mainly removed into the TL during the treatment. The monolignol in untreated CS was mainly connected by β–O–4 linkages (90.3%). Furthermore, less than 10% C—C bonds (6.3% β–β and 2.8% β–5) existed in the untreated CS lignin. After the treatment, the removed lignin in TL contained 77.9% β–O–4 linkages, 14.2% β–β bonds, and 7.9% β–5 bonds, suggesting that the treatment mainly cleaved the sensitive aryl ether to release the mobile lignin. Therefore, the acid-catalyzed thermal treatment completely deconstructed the micromolecular lignin and partially depolymerized the macromolecular lignin with G units mainly by cleaving the sensitive aryl ether.

Generally, the depolymerized lignin fragments become mobile and expand within the cell wall matrix, when the heating temperature exceeds the glass temperature. Then, the hydrophobic groups drive the lignin to aggregate onto the hydrophobic faces of the crystalline cellulose in the aqueous phase, resulting in inefficient delignification (Fig. 2). In this study, THF molecules and H_2O molecules spontaneously phase separated on the surface of lignocellulose (Mostofian et al., 2016). The THF binds to the hydrophobic surfaces, inevitably blocking the hydrophobic aggregation of lignin on the same surfaces. Alternatively, the lignin molecules dissolve into the THF–H_2O co-solvent system. The chemical composition analysis (Fig. 2) indicated that almost all the lignin (95.6%) in CS was removed in the THF-H_2O system. Additionally, the lignin-related absorption peaks of treated CS residue in the FTIR spectra (Fig. S2), including aromatic skeletal vibrations at 1513 cm^{-1}, aromatic skeletal vibrations combined with C—H in-plane deformation at 1420 cm^{-1}, C—H asymmetric deformation at 1460 cm^{-1}, and S unit breathing with C═O stretching and condensed G rings at 1329 cm^{-1} disappeared. It well confirmed that the acid-catalyzed thermal treatment efficiently removed the lignin fraction from the lignocellulose matrix.

3.2. High cellulose retention in treatment

In thermochemical treatment, cellulose and hemicellulose can be hydrolyzed via cleavage of glycosidic bonds (Rajinipriya et al., 2018). Herein, 78.5% of hemicellulose and 6.9% of glucan were hydrolyzed by the solo sulfuric acid treatment, resulting in the treated CS containing 56.6% glucan and 14.4% hemicellulose (Fig. 2). When THF is added into the treatment system, the THF and H_2O phases separate on the cellulose surface. It involves the stacking of the THF molecules on the hydrophobic areas and hydrogen bonding of water molecules with the hy-

drophilic faces (Mostofian et al., 2016). The excess water molecules are removed from the hydrophobic surfaces. However, the remaining water molecules form stronger hydrogen bonds with the oxygens of the glycosidic linkages, enhancing the hydrolytic cleavage and promoting the polysaccharides hydrolysis. Meanwhile, the amorphous hemicellulose and amorphous regions of the cellulose were primarily and easily decomposed owing to steric hindrance and kinetic forces. Consequently, in the acid-catalyzed THF-H_2O treatment, a total of 89.1% of the hemicellulose was decomposed (Fig. 2) to substantially release xylose and arabinose (Fig. S3) via acidolysis. Fewer glucan (less than 15%, Fig. 2) was hydrolyzed to release a small amount of glucose, which exhibited a weak absorption peak in the chromatogram (Fig. S3) obtained by high-performance liquid chromatography (HPLC). The hydrolysate glucose was primarily liberated from the amorphous segments of the cellulose, which was well verified by the XRD results (Fig. S4). Due to the removal of the amorphous segments, the crystallinity index of the treated CS significantly increased to 1.03 compared with that of natural CS (0.43). After the acid-catalyzed THF-H_2O treatment, the obtained CS residues have high cellulose retention, which contain 80.3% glucan, 11.2% hemicellulose, and only 1.61% lignin. Accordingly, in the FTIR spectra (Fig. S2), the absorption intensity of CH_2 stretching at 2929 cm^{-1}, CH_2 scissoring in cellulose at 1427 cm^{-1}, anti-symmetrical bridge glucosidic C—O—C stretching at 1161 cm^{-1}, C—O stretching in cellulose at 1056 cm^{-1}, and β-linkage of cellulose at 898 cm^{-1}, the characteristic absorption peaks of cellulose (Abidi et al., 2014) significantly increased.

In summary, in the THF–H_2O co-solvent system, the deconstruction of micromolecular lignin and partially depolymerization of macromolecular lignin resulted in delignification. The phase separation of THF–H_2O co-solvent concurrently blocked the hydrophobic aggregation of lignin and enhanced the hydrolysis of amorphous polysaccharide to achieve high efficiency in both delignification and cellulose retention. Consequently, the lignin stream and relatively pure cellulosic residues were synchronously obtained.

3.3. Microfibrillated celluloses (MFCs) liberation

Natural CS powders exhibit a regular and compact surface in Fig. 3a. After the acid-catalyzed THF–H_2O co-solvent system treatment, the surface becomes loose and corrugated (Fig. 3b). Some fibrous structures appear to be peeled from the surface. As the nanoscale units of cellulosic fibers, cellulose microfibrils form bundles in parallel and are embedded in the matrix of intricate hemicellulose and lignin. The natural lignocellulose exhibits great potential to be deconstructed to liberate MFCs once both lignin and hemicellulose are removed. As the analysis above, these loose and corrugated CR residues possess relatively pure cellulosic structure. Then after the ultrasonication, slender fibrils with diameters of approximately 150 nm, as presented in SEM images (Fig. 3c-d) are achieved. Integrally, the slender fibrils form a highly interlaced and web-like structure, which is consistent with the typical MFCs. During the process of ultrasonication (Fig. 4, Line 1), the ultrasound-caused small gas bubbles in the pure cellulose aqueous suspension grew rapidly via absorbing energy from the sound waves under high ultrasound intensity. Once the cavity overgrew, implosion of the cavity introduced shock waves and rapidly increasing pressure, directly causing a split in the pure cellulose fibers along the axial direction (Lu et al., 2013). Therefore, after the efficient removal of the lignin and hemicellulose, MFCs can be liberated from the integral cellulose bundles in the CS residue through the sonification by breaking the relatively weak Van der Waals force and interfibrillar hydrogen bonding.

Natural cellulose (cellulose I) generally contains two types of crystalline forms designated I_α and I_β (Atalla and Vanderhart, 1984). The peaks at 15.4° and 22.5° (Fig. S5, X-ray diffraction pattern) were assigned to the (101) and (002) plane of cellulose I_α and cellulose I_β, which were ascribed to triclinic unit cells and monoclinic type of unit cells, respectively. These results demonstrate that the cellulose I structure was not altered during the liberation of the MFCs from the CS cellulose. As displayed in the FTIR spectrum (Fig. S6), the peak around 3420 cm^{-1} is assigned to the hydrogen-bonded OH stretching. The stretching of CH_2 and C═O respond at 2929 cm^{-1} and 1650 cm^{-1}, respectively. The bands at 1427 cm^{-1} and 1161 cm^{-1} describe the CH_2 scissoring and C—O stretching in cellulose, respectively. Anti-symmetrical bridge glucosidic C—O—C stretching appears at 1161 cm^{-1}, and the β-linkage of cellulose is clearly seen at 898 cm^{-1}. All the typical absorption peaks of cellulose retain in the MFCs. Thus, the MFCs liberated from natural CS retains the typical cellulose I structure.

3.4. Lignin nanoparticles (LNPs) formation

In the purely aqueous system of the lignocellulose acid treatment, the dissociative lignin generally deposits on the hydrophobic faces of cellulose fibers. When THF was added, the preferentially stacking of THF on the same faces of the cellulose promotes lignin solvation. Then, the lignin-enriched streams were achieved. The absorption peak of the dissolved lignin in the UV-vis spectra (Fig. S7) shows a slight blueshift from 280 nm to 276 nm as compared with alkali lignin. It suggests that the THF-dissolved lignin has strong π–π stacking among the aromatic groups, which can result in spontaneous aggregation to form a micelle core with the water dilution (Fig. 4, Line 2) (Jin et al., 2001; Qian et al., 2014). With the observation of SEM (Fig. 5), uniformly spherical nanoparticles were obtained. Once the LNPs were formed, the absorption peak in the UV–vis spectra shifted back to 280 nm (Fig. S7). It indicated that a spherical-shaped arrangement of the LNPs was obtained via a self-assembly based on π-π interactions (Qian et al., 2014; Xiong et al., 2017). Therefore, THF-dissolved lignin from the natural CS formed the LNPs via self-assembly based on π-π interactions.

The obtained colloid LNPs could be easily separated by high-speed centrifugation (24,000 *g*), and controlled within nanoscale (Z-average: 102 nm, Fig. S8) and high monodispersity (PDI: 0.213). The structure of LNPs was evaluated via XPS, HSQC, FTIR, and ^{31}P-NMR. Surface composition analysis by XPS (Fig. S9 and Table 2) shows that LNPs contain 77.94 at.% carbon and 22.06 at.% oxygen. The results of energy dispersive X-ray spectrum (EDS, Fig. S10) confirmed that carbon and oxygen atom in a C/O ratio of 3.53 is present in LNPs. Hereinto, the peaks at 284.8, 286.3, and 288.1 eV in the C 1s spectrum are assigned to C—C, C—O,

and C═O, respectively. The O 1s peaks at 532.8 and 531.3 eV are associated with oxygen in the states of C—OH/C—O—C and C═O, respectively (Li et al., 2017). As listed in the Table 2, LNPs consist of 65.4% C—C type, 27.7% C—O type, and 6.9% C═O type carbon atoms. It indicated that the LNPs possessed high C—C linkages, which were considered to have higher bond energy (Ma et al., 2019; Si et al., 2018a) and greatly improve the stability of the LNPs. The LNPs structural information obtained from the HSQC spectra are shown in Fig. 1 and Table 2. The LNPs exhibit a typical hydroxy – guaiacyl – syringyl (HGS)-type lignin structure with a S/G/H ratios of 0.86/1/0.53. The preceding analysis demonstrates that the acid-catalyzed thermal treatment mainly cleaves *β*–O–4 ethers to remove the G-type lignin, which causes LNPs to contain more G units and C—C bonds (14.2% *β*–*β* bonds and 7.9% *β*–5 bonds) than the natural lignin in CS. Generally, the C—C linkages are more resistant than the aryl ether to chemical deconstruction (Gabov et al., 2014). Due to the availability of the C5 position for coupling, lignins incorporating G units contain more resistant bonds than lignins with high S unit content. Therefore, the obtained LNPs possess high structural stability, which showed great potential for composite material preparation and application. The functional groups of LNPs were detected by FTIR and ^{31}P-NMR. The absorption at 1605, 1513, and 1425 cm^{-1} (Fig. S11) in the FTIR spectrum are attributed to aromatic skeletal vibrations, well confirming the aromatic skeleton configuration of the as-prepared LNPs. The strong absorption at 3420 cm^{-1} in the FTIR spectra suggests that LNPs have a typical polyhydroxy structure. Furthermore, the ^{31}P-NMR spectrum (Fig. S12) confirms that the hydroxyl groups of the LNPs include aliphatic OH, G, H, and S phenolic units, which could be regarded as the active sites to introduce new functional groups onto LNPs and create new functional polymer composites (Dai et al., 2017; Sipponen et al., 2017). Thus, the THF-dissolved lignin formed monodisperse LNPs with high structural stability and functional groups in the co-solvent system.

3.5. Carbon quantum dots (CQDs) formation

Uniform 3–4 nm nanodots (Fig. 6a, Fig. S13) were also observed after the separation of LNPs from the treatment liquor. The lattice spacing (Fig. 6b) of 0.25 nm, corresponding to the (100) diffraction facets of graphitic carbon (Baker and Baker, 2010), observed in the high-magnification TEM image suggests that the CQDs have a crystalline structure. Furthermore, the obscure peaks at 1360 and 1590 cm^{-1} (Fig. S14), which attributed to the D and G bands of carbon materials, respectively, in the Raman spectrum (Fig. S15) confirm that the crystalline CQDs possess graphitic sp^2 carbon atoms and sp^3 carbon defects. Surface composition analysis by XPS (Fig. S16) shows 63.82 at.% carbon, 27.44 at.% oxygen, and 8.73 at.% nitrogen contains in the CQDs. Hereinto, three different types of carbon atoms are present: sp^3 for aliphatic and sp^2 for graphitic (C—C at 284.6 eV and C═C at 284.1 eV), oxygenated (C—O at 286.4 eV and C═O at 287.9 eV), and nitrous (C—N at 285.8 eV) (Zhang et al., 2019). The O 1s peaks at 533.0 and 531.8 eV are associated with oxygen in the states of C—OH/C—O—C and C═O, respectively. The peaks at 399.4, 400.1, and 401.1 eV in the N 1s spectrum are assigned to C—N—C, N—$(C)_3$ and N—H, respectively (Zhang et al., 2018b). Therefore, the as-synthesized CQDs can be classified as N-doped, carbon-rich nanodots. The aqueous dispersions of the CQDs exhibits obvious emission peaks, which hardly shift at the wavelengths of 410 nm with the increasing excitation wavelengths from 500 to 700 nm significant upconversion. Besides, the change of zeta potential from 17.1 mV to -35.6 mV with the pH increasing from 1.8 to 11.1 (Fig. S17). The results above suggest that the CQDs are amphoteric and possess significant upconversion PL properties. In the acid-catalyzed hydrothermal system (Fig. 2, Line 3), monosaccharides, organic acids, and benzene compounds were released by acidolysis. These compounds are thermally converted into polymeric products through dehydration, polymerization, and condensation. Sequentially, they underwent aromatization and carbonization via condensation and cycloaddition reactions. Once the concentration reached a critical supersaturation point, these aromatic clusters developed into CQDs via burst nucleation (Si et al., 2018b). In addition, peptides originating from thermally denatured protein in the corn stover contribute to the N-doping via carbonization and oxidation of the polymeric products.

4. Conclusions

The heterogeneous structure of lignocellulose is kinetically challenged to fabricate bio-nanomaterials. Based on the lignocellulosic structure and phase separation of co-solvent, an acid-catalyzed THF–H_2O co-solvent system was employed. This work efficiently integrates three types of lignocellulose-based nanomaterial preparation, including MFCs, LNPs and CQDs, into an integrated pathway. Lignin was removed to form LNPs via π–π interactions. The MFCs were liberated from the cellulose bundles. Simultaneously, the released monomolecular compounds, which served as precursors, were thermally processed for CQDs production. The integrated pathway provides a novel route for bio-nanomaterial preparation and promotes the industrialization process of the bio-nanomaterials.

CRediT authorship contribution statement

Mengying Si: Conceptualization, Methodology, Investigation, Visualization, Writing - original draft. **Mika Sillanpää:** Validation, Writing - review & editing. **Shengnan Zhuo:** Methodology, Investigation, Formal analysis. **Jin Zhang:** Investigation, Validation. **Mingren Liu:** Methodology. **Sheng Wang:** Visualization. **Congjie Gao:** Supervision. **Liyuan Chai:** Supervision, Project administration. **Feiping Zhao:** Writing - review & editing. **Yan Shi:** Conceptualization, Resources, Writing - review & editing, Supervision.

Declaration of Competing Interest

None.

Acknowledgments

This work was supported by the National Key R&D Program of China (2017YFC0210400), the key project of National Natural Science Foundation of China (51634010), and the Key R&D Program of Hunan Province (2018SK2044).

Appendix A. Supplementary data

Supplementary material related to this article can be found, in the online version, at doi:https://doi.org/10.1016/j.indcrop.2020.112469.

References

Abdul Khalil, H.P.S., Bhat, A.H., Ireana Yusra, A.F., 2012. Green composites from sustainable cellulose nanofibrils: a review. Carbohydr. Polym. 87 (2), 963–979. https://doi.org/10.1016/j.carbpol.2011.08.078.

Abidi, N., Cabrales, L., Haigler, C.H., 2014. Changes in the cell wall and cellulose content of developing cotton fibers investigated by FTIR spectroscopy. Carbohydr. Polym. 100, 9–16. https://doi.org/10.1016/j.carbpol.2013.01.074.

Ago, M., Huan, S., Borghei, M., Raula, J., Kauppinen, E.I., Rojas, O.J., 2016. High-throughput synthesis of lignin particles (~ 30 nm to ~2 μm) via aerosol flow reactor: size fractionation and utilization in Pickering emulsions. ACS Appl. Mater. Interfaces 8 (35), 23302–23310. https://doi.org/10.1021/acsami.6b07900.

Almeida, A.P.C., Canejo, J.P., Fernandes, S.N., Echeverria, C., Almeida, P.L., Godinho, M.H., 2018. Cellulose-based biomimetics and their applications. Adv. Mater. 30 (19), e1703655https://doi.org/10.1002/adma.201703655.

Atalla, R., DL, V., 1984. Native cellulose - a composite of two distinct crystalline forms. Science 223, 283–285.

Atalla, R.H., Vanderhart, D.L., 1984. Native cellulose: a composite of two distinct crystalline forms. Science 223 (4633), 283–285. https://doi.org/10.1126/science.223.4633.283.

Baker, S.N., Baker, G.A., 2010. Luminescent carbon nanodots: emergent nanolights. Angew. Chem. Int. Ed. 49 (38), 6726–6744. https://doi.org/10.1002/anie.200906623.

Cai, Y., Zhang, K., Kim, H., Hou, G., Zhang, X., Yang, H., Feng, H., Miller, L., Ralph, J., Liu, C.J., 2016. Enhancing digestibility and ethanol yield of Populus wood via expression of an engineered monolignol 4-O-methyltransferase. Nat. Commun. 7, 11989. https://doi.org/10.1038/ncomms11989.

Dai, L., Liu, R., Hu, L.-Q., Zou, Z.-F., Si, C.-L., 2017. Lignin nanoparticle as a novel green carrier for the efficient delivery of resveratrol. ACS Sustain. Chem. Eng. 5 (9), 8241–8249. https://doi.org/10.1021/acssuschemeng.7b01903.

Dai, Y., Si, M., Chen, Y., Zhang, N., Zhou, M., Liao, Q., Shi, D., Liu, Y., 2015. Combination of biological pretreatment with NaOH/Urea pretreatment at cold temperature to enhance enzymatic hydrolysis of rice straw. Bioresour. Technol. 198, 725–731. https://doi.org/10.1016/j.biortech.2015.09.091.

Ding, S.-Y., Himmel, M.E., 2006. The maize primary cell wall microfibril: a new model derived from direct visualization. J. Agric. Food Chem. 54, 597–606.

Donohoe, B.S., Decker, S.R., Tucker, M.P., Himmel, M.E., Vinzant, T.B., 2008. Visualizing lignin coalescence and migration through maize cell walls following thermochemical pretreatment. Biotechnol. Bioeng. 101 (5), 913–925. https://doi.org/10.1002/bit.21959.

Dou, J., Bian, H., Yelle, D.J., Ago, M., Vajanto, K., Vuorinen, T., Zhu, J., 2019. Lignin containing cellulose nanofibril production from willow bark at 80 °C using a highly recyclable acid hydrotrope. Ind. Crop. Prod. 129, 15–23. https://doi.org/10.1016/j.indcrop.2018.11.033.

Figueiredo, P., Lintinen, K., Hirvonen, J.T., Kostiainen, M.A., Santos, H.A., 2018. Properties and chemical modifications of lignin: towards lignin-based nanomaterials for biomedical applications. Prog. Mater. Sci. 93, 233–269. https://doi.org/10.1016/j.pmatsci.2017.12.001.

Gabov, K., Gosselink, R.J., Smeds, A.I., Fardim, P., 2014. Characterization of lignin extracted from birch wood by a modified hydrotropic process. J. Agric. Food Chem. 62 (44), 10759–10767. https://doi.org/10.1021/jf5037728.

Guidetti, G., Atifi, S., Vignolini, S., Hamad, W.Y., 2016. Flexible photonic cellulose nanocrystal films. Adv. Mater. 28 (45), 10042–10047. https://doi.org/10.1002/adma.201603386.

Jia, C., Chen, C., Kuang, Y., Fu, K., Wang, Y., Yao, Y., Kronthal, S., Hitz, E., Song, J., Xu, F., Liu, B., Hu, L., 2018. From wood to textiles: top-down assembly of aligned cellulose nanofibers. Adv. Mater. 30 (30), e1801347https://doi.org/10.1002/adma.201801347.

Jin, J., Iyoda, T., Cao, C., Song, Y., Jiang, L., Li, T.J., Zhu, D.B., 2001. Self-assembly of uniform spherical aggregates of magnetic nanoparticles through π-π interactions. Angew. Chem. Int. Ed. 40 (11), 2135–2138. https://doi.org/10.1002/1521-3773(20010601)40:11<2135::AID-ANIE2135>3.3.CO;2-F.

Kai, D., Tan, M.J., Chee, P.L., Chua, Y.K., Yap, Y.L., Loh, X.J., 2016. Towards lignin-based functional materials in a sustainable world. Green Chem. 18 (5), 1175–1200. https://doi.org/10.1039/c5gc02616d.

Kontturi, E., Laaksonen, P., Linder, M.B., Nonappa, Groschel, A.H., Rojas, O.J., Ikkala, O., 2018. Advanced materials through assembly of nanocelluloses. Adv. Mater. 30 (24), e1703779https://doi.org/10.1002/adma.201703779.

Li, Y., Zhou, M., Pang, Y., Qiu, X., 2017. Lignin-based microsphere: preparation and performance on encapsulating the pesticide avermectin. ACS Sustain. Chem. Eng. 5 (4), 3321–3328. https://doi.org/10.1021/acssuschemeng.6b03180.

Lim, S.Y., Shen, W., Gao, Z., 2015. Carbon quantum dots and their applications. Chem. Soc. Rev. 44 (1), 362–381. https://doi.org/10.1039/c4cs00269e.

Linger, J.G., Vardon, D.R., Guarnieri, M.T., Karp, E.M., Hunsinger, G.B., Franden, M.A., Johnson, C.W., Chupka, G., Strathmann, T.J., Pienkos, P.T., Beckham, G.T., 2014. Lignin valorization through integrated biological funneling and chemical catalysis. Proc. Natl. Acad. Sci. U. S. A. 111 (33), 12013–12018. https://doi.org/10.1073/pnas.1410657111.

Lintinen, K., Xiao, Y., Bangalore Ashok, R., Leskinen, T., Sakarinen, E., Sipponen, M., Muhammad, F., Oinas, P., Österberg, M., Kostiainen, M., 2018. Closed cycle production of concentrated and dry redispersible colloidal lignin particles with a three solvent polarity exchange method. Green Chem. 20 (4), 843–850. https://doi.org/10.1039/c7gc03465b.

Lu, Y., Sun, Q., She, X., Xia, Y., Liu, Y., Li, J., Yang, D., 2013. Fabrication and characterisation of alpha-chitin nanofibers and highly transparent chitin films by pulsed ultrasonication. Carbohydr. Polym. 98 (2), 1497–1504. https://doi.org/10.1016/j.carbpol.2013.07.038.

Lynd, L.R., Laser, M.S., Bransby, D., Dale, B.E., Davison, B., Hamilton, R., Himmel, M., Keller, M., McMillan, J.D., Sheehan, J., Wyman, C.E., 2008. How biotech can transform biofuels. Nat. Biotechnol. 26, 169–172.

Lynd, L.R., Liang, X., Biddy, M.J., Allee, A., Cai, H., Foust, T., Himmel, M.E., Laser, M.S., Wang, M., Wyman, C.E., 2017. Cellulosic ethanol: status and innovation. Curr. Opin. Biotechnol. 45, 202–211. https://doi.org/10.1016/j.copbio.2017.03.008.

Ma, M., Dai, L., Si, C., Hui, L., Liu, Z., Ni, Y., 2019. A facile preparation of super long-term stable lignin nanoparticles from black liquor. ChemSusChem 12, 5216. https://doi.org/10.1002/cssc.201903230.

Moon, R.J., Martini, A., Nairn, J., Simonsen, J., Youngblood, J., 2011. Cellulose nanomaterials review: structure, properties and nanocomposites. Chem. Soc. Rev. 40 (7), 3941–3994. https://doi.org/10.1039/c0cs00108b.

Mostofian, B., Cai, C.M., Smith, M.D., Petridis, L., Cheng, X., Wyman, C.E., Smith, J.C., 2016. Local phase separation of co-solvents enhances pretreatment of biomass for bioenergy applications. J. Am. Chem. Soc. 138 (34), 10869–10878. https://doi.org/10.1021/jacs.6b03285.

Nguyen, T.Y., Cai, C.M., Kumar, R., Wyman, C.E., 2015. Co-solvent pretreatment reduces costly enzyme requirements for high sugar and ethanol yields from lignocellulosic biomass. Chemsuschem 8 (10), 1716–1725. https://doi.org/10.1002/cssc.201403045.

Nguyen, T.Y., Cai, C.M., Kumar, R., Wyman, C.E., 2017. Overcoming factors limiting high-solids fermentation of lignocellulosic biomass to ethanol. Proc. Natl. Acad. Sci. U. S. A. 114 (44), 11673–11678. https://doi.org/10.1073/pnas.1704652114.

Nguyen, T.Y., Cai, C.M., Osman, O., Kumara, R., Wyman, C.E., 2016. CELF pretreatment of corn stover boosts ethanol titers and yields from high solids SSF with low enzyme loadings. Green Chem. 18, 1581–1589. https://doi.org/10.1039/c5gc01977j.

Niu, N., Ma, Z., He, F., Li, S., Li, J., Liu, S., Yang, P., 2017. Preparation of carbon dots for cellular imaging by the molecular aggregation of cellulolytic enzyme lignin. Langmuir 33 (23), 5786–5795. https://doi.org/10.1021/acs.langmuir.7b00617.

Parker, R.M., Guidetti, G., Williams, C.A., Zhao, T., Narkevicius, A., Vignolini, S., Frka-Petesic, B., 2018. The self-assembly of cellulose nanocrystals: hierarchical design of visual appearance. Adv. Mater. 30 (19), 1704477https://doi.org/10.1002/adma.201704477.

Qian, Y., Deng, Y., Qiu, X., Li, H., Yang, D., 2014. Formation of uniform colloidal spheres from lignin, a renewable resource recovered from pulping spent liquor. Green Chem. 16 (4), 2156–2163. https://doi.org/10.1039/c3gc42131g.

Ragauskas, A.J., Beckham, G.T., Biddy, M.J., Chandra, R., Chen, F., Davis, M.F., Davison, B.H., Dixon, R.A., Gilna, P., Keller, M., Langan, P., Naskar, A.K., Saddler, J.N., Tschaplinski, T.J., Tuskan, G.A., Wyman, C.E., 2014. Lignin valorization: improving lignin processing in the biorefinery. Science 344 (6185), 1246843https://doi.org/10.1126/science.1246843.

Rajinipriya, M., Nagalakshmaiah, M., Robert, M., Elkoun, S., 2018. Importance of agricultural and industrial waste in the field of nanocellulose and recent industrial developments of wood based nanocellulose: a review. ACS Sustain. Chem. Eng. 6 (9), 2807–2828.

Richter, A.P., Brown, J.S., Bharti, B., Wang, A., Gangwal, S., Houck, K., Cohen Hubal, E.A., Paunov, V.N., Stoyanov, S.D., Velev, O.D., 2015. An environmentally benign antimicrobial nanoparticle based on a silver-infused lignin core. Nat. Nanotechnol. 10 (9), 817–823. https://doi.org/10.1038/nnano.2015.141.

Segal, L., 1959. An empirical method for estimating the degree of crystallinity of native cellulose using the X-ray diffractometer. Text. Res. J. 29 (10), 786–794. https://doi.org/10.1177/004051755902901003.

Sen, S., Patila, S., Argyropoulos, D.S., 2015. Thermal properties of lignin in copolymers, blends, and composites: a review. Green Chem. 17, 4862–4887. https://doi.org/10.1039/c5gc01066g.

Shi, Y., Chai, L., Tang, C., Yang, Z., Zhang, H., Runhua, C., Chen, Y., Zheng, Y., 2013. Characterization and genomic analysis of kraft lignin biodegradation by the beta-proteobacterium Cupriavidus basilensis B-8. Biotechnol. Biofuel. 6 (1), 2–14.

Si, M., Liu, D., Liu, M., Yan, X., Gao, C., Chai, L., Shi, Y., 2019. Complementary effect of combined bacterial-chemical pretreatment to promote enzymatic digestibility of lignocellulose biomass. Bioresour. Technol. 272, 272–280. https://doi.org/10.1016/j.biortech.2018.10.036.

Si, M., Yan, X., Liu, M., Shi, M., Wang, Z., Wang, S., Zhang, J., Gao, C., Chai, L., Shi, Y., 2018. In situ lignin bioconversion promotes complete carbohydrate conversion of rice straw by Cupriavidus basilensis B-8. ACS Sustain. Chem. Eng. 6 (6), 7969–7978. https://doi.org/10.1021/acssuschemeng.8b01336.

Si, M., Zhang, J., He, Y., Yang, Z., Yan, X., Liu, M., Zhuo, S., Wang, S., Min, X., Gao, C., Chai, L., Shi, Y., 2018. Synchronous and rapid preparation of lignin nanoparticles and carbon quantum dots from natural lignocellulose. Green Chem. 20 (15), 3414–3419. https://doi.org/10.1039/c8gc00744f.

Sipponen, M.H., Smyth, M., Leskinen, T., Österberg, M., 2017. All-lignin approach to prepare cationic colloidal lignin particles_ Stabilization of durable Pickering emulsions. Green Chem. 19, 5831–5840. https://doi.org/10.1039/c7gc02900d.

Teramoto, Y., Tanaka, N., Lee, S.H., Endo, T., 2008. Pretreatment of eucalyptus wood chips for enzymatic saccharification using combined sulfuric acid-free ethanol cooking and ball milling. Biotechnol. Bioeng. 99 (1), 75–85. https://doi.org/10.1002/bit.21522.

Thakur, V.K., Thakur, M.K., Raghavan, P., Kessler, M.R., 2014. Progress in green polymer composites from lignin for multifunctional applications: a review. ACS Sustain. Chem. Eng. 2 (5), 1072–1092. https://doi.org/10.1021/sc500087z.

Thomas, B., Raj, M.C., B, A.K, H, R.M., Joy, J., Moores, A., Drisko, G.L., Sanchez, C., 2018. Nanocellulose, a versatile green platform: from biosources to materials and their applications. Chem. Rev. 118 (24), 11575–11625. https://doi.org/10.1021/acs.chemrev.7b00627.

Wang, J., Wang, C.-F., Chen, S., 2012. Amphiphilic egg-derived carbon dots: rapid plasma fabrication, pyrolysis process, and multicolor printing patterns. Angew. Chem. Int. Ed. 124, 9451–9455. https://doi.org/10.1002/anie.

Wen, J.-L., Sun, S.-L., Yuan, T.-Q., Sun, R.-C., 2015. Structural elucidation of whole lignin from Eucalyptus based on preswelling and enzymatic hydrolysis. Green Chem. 17 (3), 1589–1596. https://doi.org/10.1039/c4gc01889c.

Xiong, F., Han, Y., Wang, S., Li, G., Qin, T., Chen, Y., Chu, F., 2017. Preparation and formation mechanism of size-controlled lignin nanospheres by self-assembly. Ind. Crop. Prod. 100, 146–152. https://doi.org/10.1016/j.indcrop.2017.02.025.

Yang, Z.C., Wang, M., Yong, A.M., Wong, S.Y., Zhang, X.H., Tan, H., Chang, A.Y., Li, X., Wang, J., 2011. Intrinsically fluorescent carbon dots with tunable emission derived from hydrothermal treatment of glucose in the presence of monopotassium phosphate. Chem. Commun. 47 (42), 11615–11617. https://doi.org/10.1039/c1cc14860e.

Zhang, J., Yan, M., Yuan, X., Si, M., Jiang, L., Wu, Z., Wang, H., Zeng, G., 2018. Nitrogen doped carbon quantum dots mediated silver phosphate/bismuth vanadate Z-scheme photocatalyst for enhanced antibiotic degradation. J. Colloid Interface Sci. 529, 11–22. https://doi.org/10.1016/j.jcis.2018.05.109.

Zhang, J., Yuan, X., Jiang, L., Wu, Z., Chen, X., Wang, H., Wang, H., Zeng, G., 2018. Highly efficient photocatalysis toward tetracycline of nitrogen doped carbon quantum dots sensitized bismuth tungstate based on interfacial charge transfer. J. Colloid Interface Sci. 511, 296–306. https://doi.org/10.1016/j.jcis.2017.09.083.

Zhang, K., Liimatainen, H., 2018. Hierarchical assembly of nanocellulose-based filaments by interfacial complexation. Small 14 (38), e1801937https://doi.org/10.1002/smll.201801937.

Zhang, K., Liu, M., Si, M., Wang, Z., Zhuo, S., Chai, L., Shi, Y., 2019. Polyhydroxyalkanoate-modified bacterium regulates biomass structure and promotes synthesis of carbon materials for high-performance supercapacitors. ChemSusChem 12 (8), 1732–1742. https://doi.org/10.1002/cssc.201802894.

Zhang, L., Yan, L., Wang, Z., Laskar, D.D., Swita, M.S., Cort, J.R., Yang, B., 2015. Characterization of lignin derived from water-only and dilute acid flowthrough pretreatment of poplar wood at elevated temperatures. Biotechnol. Biofuel. 8, 203. https://doi.org/10.1186/s13068-015-0377-x.

Zhang, X., Jiang, M., Niu, N., Chen, Z., Li, S., Liu, S., Li, J., 2018. Natural-product-derived carbon dots: from natural products to functional materials. ChemSusChem 11 (1), 11–24. https://doi.org/10.1002/cssc.201701847.

Zhao, W., Simmons, B., Singh, S., Ragauskas, A., Cheng, G., 2016. From lignin association to nano-/micro-particle preparation: extracting higher value of lignin. Green Chem. 18 (21), 5693–5700. https://doi.org/10.1039/c6gc01813k.

Zhu, H., Luo, W., Ciesielski, P.N., Fang, Z., Zhu, J.Y., Henriksson, G., Himmel, M.E., Hu, L., 2016. Wood-derived materials for green electronics, biological devices, and energy applications. Chem. Rev. 116 (16), 9305–9374. https://doi.org/10.1021/acs.chemrev.6b00225.